Heterogeneous Catalysis Hot Paper

DOI: 10.1002/ange.201409333

Heterogeneous Water Oxidation: Surface Activity versus Amorphization Activation in Cobalt Phosphate Catalysts**

Diego González-Flores, Irene Sánchez, Ivelina Zaharieva, Katharina Klingan, Jonathan Heidkamp, Petko Chernev, Prashanth W. Menezes, Matthias Driess, Holger Dau, and Mavis L. Montero**

Dedicated to Professor Herbert W. Roesky

Abstract: *Is water oxidation catalyzed at the surface or within the bulk volume of solid oxide materials? This question is addressed for cobalt phosphate catalysts deposited on inert electrodes, namely crystallites of pakhomovskyite ($Co_3(PO_4)_2{\cdot}8H_2O$, Pak) and phosphate-containing Co oxide (CoCat). X-ray spectroscopy reveals that oxidizing potentials transform the crystalline Pak slowly (5–8 h) but completely into the amorphous CoCat. Electrochemical analysis supports high-TOF surface activity in Pak, whereas its amorphization results in dominating volume activity of the thereby formed CoCat material. In the directly electrodeposited CoCat, volume catalysis prevails, but not at very low levels of the amorphous material, implying high-TOF catalysis at surface sites. A complete picture of heterogeneous water oxidation requires insight in catalysis at the electrolyte-exposed "outer surface", within a hydrated, amorphous volume phase, and modes and kinetics of restructuring upon operation.*

Water oxidation is a pivotal step in the environmentally friendly production of hydrogen or low-carbon-based fuels.[1] However, the design and implementation of a stable catalytic system for efficient water oxidation operating at high catalytic turnover frequency (TOF) and number (TON), with low activation barrier, moderate overpotential, and high current density is a challenging hurdle along the way.[2] In this pursuit, water oxidation (or oxygen evolution reaction, OER) in the neutral pH regime catalyzed by oxide materials based on the earth-abundant transition metals is of high interest. In particular, amorphous cobalt-based oxide catalysts (CoCat) have been extensively investigated regarding (electro)synthesis and self-repair,[3] atomic structure,[4] and electrokinetic properties,[5] as reviewed elsewhere.[6]

Aiming at rationale development of improved catalysts, one of the basic questions awaiting clarification is the role of surface catalysis versus catalysis within the bulk volume of a solid-state material. Water oxidation by heterogeneous catalysts consisting of (aggregated) crystallites of micro- or nanometer dimensions on electrode surfaces mostly is discussed in terms of catalysis happening at crystallite surface sites and determined by elemental composition and atomic structure of the crystalline material.[7] On the other hand, it was recently demonstrated that for the CoCat, the bulk oxide material promotes catalysis.[8] Proton transfer to electrolyte bases becomes a co-determinant of catalytic rates at high overpotentials (high current densities), but water oxidation itself takes place in the bulk material consisting of cobalt-oxide clusters interfaced by cations (for example, potassium), anions (phosphate), and water molecules (Figure 1).[8]

In some crystalline inorganic materials, for example, perovskites[9] and $LiCoO_2$,[10] a surface reconstruction during the OER results in an amorphous layer at the crystal surface, which resembles the CoCat closely with respect to its atomic structure. Chemical oxidation of an initially catalytically inactive nanocrystalline manganese oxide (MnO) transformed the bulk of the material into an amorphous $Mn^{III/IV}$ oxide and resulted in a catalytically active material.[11] Also for prominent molecular catalysts, transformation into an amorphous oxide has been related to OER activity.[12a,b] Recently it was also shown for a heterobimetallic Co-Fe oxide system that its amorphous state surpasses the OER activity of the crystalline form.[12c] These findings raise the important question whether efficient OER catalysis by first-row transition metal is generally facilitated by amorphous oxide phases. If this were true, structure–activity relationships detected for crystalline materials would be determined by extent and rate of surface amorphization, but not by any direct influence of atomic and electronic structure of the

[*] D. González-Flores, Dr. I. Zaharieva, K. Klingan, J. Heidkamp, Dr. P. Chernev, Prof. Dr. H. Dau
Department of Physics, Freie Universität Berlin
Arnimallee 14, 14195 Berlin (Germany)
E-mail: holger.dau@fu-berlin.de

I. Sánchez, Dr. M. L. Montero
Centro de Electroquímica y Energía Química (CELEQ) and Escuela de Química, Universidad de Costa Rica
11501 2060, San José (Costa Rica)
E-mail: mavis.montero@ucr.ac.cr

Dr. P. W. Menezes, Prof. Dr. M. Driess
Department of Chemistry: Metalorganics and Inorganic Materials
Technische Universität Berlin
Strasse des 17. Juni 135, 10623 Berlin (Germany)

[**] Financial support by the Deutsche Forschungsgemeinschaft (DFG) to the SPP 1613 (DA 402/7-1), the Cluster of Excellence "Unifying Concepts in Catalysis" (UniCat, Berlin), and by CONICIT-MICIT (Costa Rica) is gratefully acknowledged. The XAS experiments were performed at the KMC1 beamline of the BESSY synchrotron operated by the Helmholtz Zentrum Berlin (HZB); we thank Dr. F. Schäfers and M. Mertin (both HZB) for support in the XAS experiment.

Supporting information for this article is available on the WWW under http://dx.doi.org/10.1002/anie.201409333.

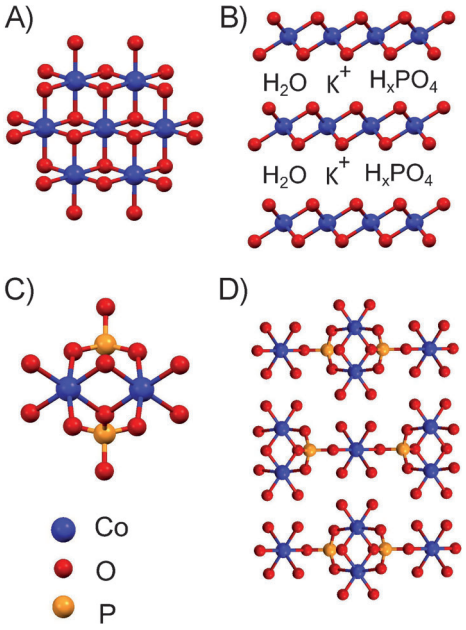

Figure 1. A) Cobalt oxo fragment of the CoCat. B) Layered structure of the CoCat with ions and water intercalated between Co oxide layers. C) Phosphate binding and μ-oxo bridging in pakhomovskyite. D) Layered structure of pakhomovskyite; the layers are joined by hydrogen bonds (not shown).

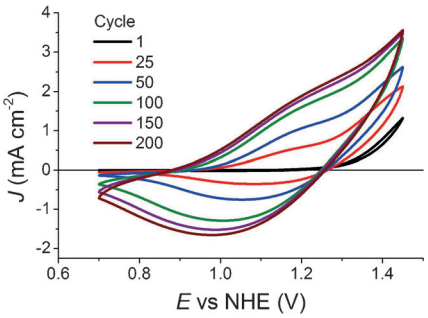

Figure 2. Series of cyclic voltammograms (CVs) of sample A deposited on FTO electrodes (*E* vs. NHE; CV with 10 mVs^{-1} in 0.1 M phosphate buffer at pH 7, 85% IR compensation).

crystalline material on the OER; the results of a significant number of investigations would be invalidated. Herein we will provide evidence for a Solomonic point of view, namely that both surface catalysis and bulk-volume catalysis can prevail, and both need to be taken into account when striving for a complete picture of heterogeneous water oxidation.

We investigated crystalline cobalt phosphate with the formula $Co_3(PO_4)_2{\cdot}8H_2O$, which is classified in the vivianite group and denoted as pakhomovskyite.[13] The relatively intricate atomic structure of pakhomovskyite (Pak) exhibits analogies to the CoCat structure (see Figure 1 and Supporting Information). Pakhomovskyite was prepared following either a previously reported precipitation procedure (sample A)[14] or a new electrosynthesis approach (sample B) described in the Experimental Section and the Supporting Information, where also elemental composition, structural characterization by X-ray diffraction analysis, and electron micrographs are documented (Table S1, Figures S1 and S2).

To investigate the electrochemical properties of pakhomovskyite, we physically deposited microcrystalline sample A and B on FTO electrodes and investigated the respective catalyst–electrode assembly in a 0.1 mol L^{-1} phosphate buffer at pH 7. Cyclic voltammograms (CVs) are shown in Figure 2. Already during the first cycle, sample A exhibits a clear catalytic wave corresponding to a catalytic current exceeding 1 mA cm^{-2}. Interestingly, the catalytic current (at 1.45 V) increases with each CV cycle. This increase is accompanied by the rise of an oxidation wave (broad peak in the CV around 1.2 V) and reduction wave (broad negative peak around 1.0 V) for cobalt oxidation and reduction, respectively; integration of the reductive currents provides a measure for the number of redox-active cobalt ions[4c,8] (the observed behavior is often discussed in terms of a pseudocapacitance[9]). The increasing redox activity is typical for amorphization processes in crystalline materials under electrochemical operation.[9,10] A very similar behavior is observed in sample B; however, its initial redox activity is higher, which is explainable by either the smaller crystallite size and thus higher surface area (Figure S2 and S3) or faster amorphization owing to the presence of calcium and sodium ions.

SEM images collected before and after catalytic operation show the transformation of small separated crystals into amorphous islands (Figure S4), confirmed also by powder XRD (Figure S5). The initially fully transparent film is transformed into a brownish material; UV/Vis spectra collected in situ during catalytic operation suggest a continuous structural transformation of the catalyst material (Figure S6 to S9). We also performed long-term electrolysis at constant anode potential (1.35 V vs. NHE), complemented by CV measurements at selected times (sample A in Figure 3, sample B in Figures S10 and S11). Starting at a low but clearly detectable level of catalytic current (for the current level within the first 2 min, see Figures S17 and S19), the current increases with time. The current increase likely relates to the increase in redox activity by the amorphization of the catalyst material (see below).

Upon exposure to catalytic potentials, catalyst activation is observed (Figure 2 and Figure 3) and changing UV/Vis spectra suggests structural changes at the atomic and electronic level (Figures S7 and S8). To understand the structural changes coupled to catalyst activation, the electrochemical experiment was combined with X-ray absorption spectroscopy (XAS) at the cobalt K-edge. We performed low-temperature XAS measurements on electrodes of sample A (Figure 4) and B (Figures S12 and S13), which were rapidly frozen before any electrochemical treatment, after 2 min, and after 10 h at 1.35 V (vs NHE). The XANES spectra (X-ray absorption near-edge structure, Figure 4A and Figure S12) show a shift in the X-ray edge position from 7717.6 to 7720.6 eV, suggesting that 10 h exposure to 1.35 V results in essentially complete conversion of the Co^{II} ions of Pak into Co^{III} ions; the Co^{III} spectra detected after 10 h resemble closely the XANES spectra of amorphous CoCat reported elsewhere.[4a] The transformation of the Pak mineral into the amorphous CoCat is confirmed by the Fourier transforms (FTs) of the extended X-ray absorption fine-structure

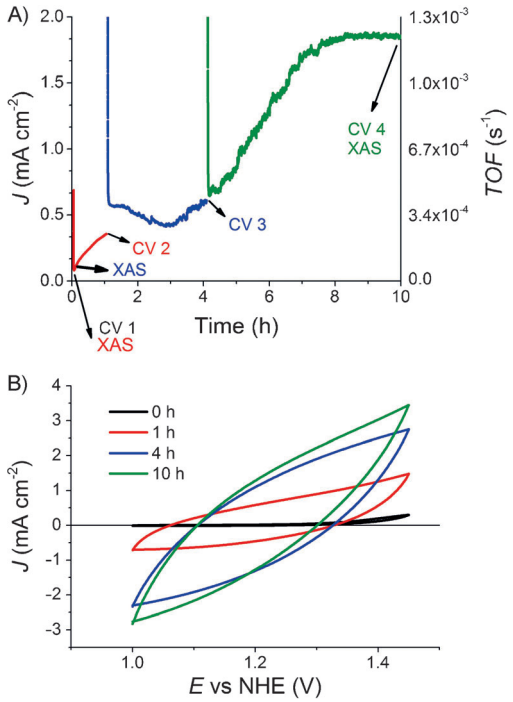

Figure 3. Long-term electrolysis for sample A applying 1.35 V vs NHE for 10 h (in 0.1 M phosphate buffer at pH 7). A) Time course of the current density. At the indicated times CV were measured and samples rapidly frozen for analysis by X-ray absorption spectroscopy. B) CVs detected at a scan rate of 20 mVs^{-1}.

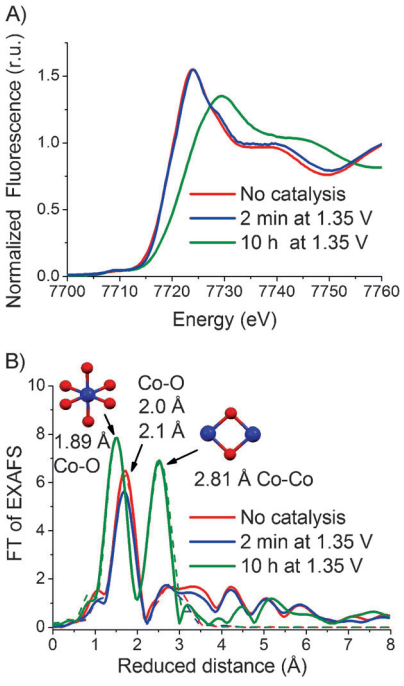

Figure 4. X-ray absorption spectra collected at the cobalt K-edge for pakhomovskyite (sample A) deposited on FTO electrodes (red lines), after exposure to 1.35 V (vs. NHE, pH 7) for 2 min (blue) and 10 h (green). A) XANES spectra. B) Fourier-transformed EXAFS spectra. The indicated reduced distance is by about 0.4 Å shorter than the precise distance obtained by EXAFS simulations. The dotted lines results from EXAFS simulations (see Table S2 for parameters).

(EXAFS) spectra (Figure 4B and Figure S13). The spectrum of the sample A before electrolysis can be modeled according to the Pak crystal structure (Supporting Information, Figure S15 and Table S2). After 10 h at 1.35 V, a Co–O distance of 1.89 Å and Co–Co distance at 2.82 Å are detectable, which are identical to the previously reported distances of the CoCat.

We conclude that long-term exposure to catalytic potential results in complete conversion of the microcrystalline Pak (Figure 1B) into the amorphous CoCat, which consists of fragments of a layered oxide with edge-sharing $Co^{III}O_6$ octahedra (Figure 1A). This conversion requires several hours as verified by XAS analysis of the Pak samples exposed to catalytic potentials for 2 min only (Figures S16–S19). The structural changes detected by XAS are compatible with the transformation of the FTIR spectra (Figures S20, S21, Table S3) and supported by highly similar catalytic properties of amorphized Pak and directly electrodeposited CoCat (Figure S28).

For the CoCat and other materials, a close relation between redox activity and catalytic activity has been reported.[4c,8] This relation was investigated for the Pak material exposed for more than 8 h to a continuous sequence of CVs. The redox activity was measured via integration of the reductive currents of the CV resulting in a redox charge, q_{red}, which provides N_{red}, the number of redox-active cobalt ions undergoing oxidation state changes ($N_{red} = q_{red}/e$).[4c,8] An initial catalytic current (about 1.3 mA in Figure 5) is clearly detectable, which is associated with a low level of redox activity. Subsequently, amorphization results in the concomitant increase of both redox and catalytic activity. The red bars in Figure 5 indicate the ratio between catalytic current and redox charge, which may be viewed as a turnover frequency per redox-active cobalt ion (TOF^q). It is clearly visible that

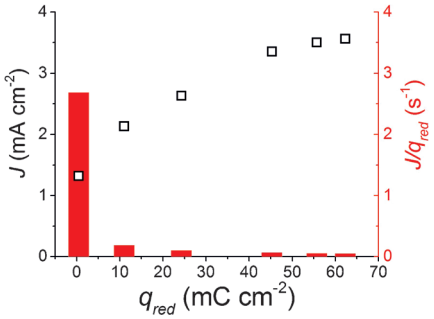

Figure 5. Relationship between redox charge (q_{red}), catalytic activity (J), and TOF per redox-active site (J/q_{red}) during Pak→CoCat conversion. The redox charge was quantified by integration of the reductive currents of the six CVs shown in Figure 2. The catalytic activity was estimated from the maximal current detected in the respective CV (at 1.45 V vs. NHE) and is indicated by open squares (left current-density axis). The red bars relate to the right y-axis and indicate the ratio between catalytic current density (J) and redox charge (q_{red}) in units of s^{-1} ($= A C^{-1}$). This ratio may be viewed as a turnover frequency (TOF^q, rate of catalytic electron flow per redox-active cobalt ion). Both q_{red} and J are normalized to the macroscopic electrode area. For better visibility of low levels of J/q_{red}, see Figure S22. For data on J/q_{red} vs. q_{red} with the catalytic currents measured in chronoamperometric experiments, see Figure S23 to S25.

the value of TOF^q is high before onset of amorphization (left red bar) and clearly lower at later times (small red bars).

We interpret the above findings as follows: In the initially crystalline material, water oxidation catalysis takes place at surface sites; the catalytic TOF per cobalt ion at the crystallite surface is high. Upon long-term operation at catalytic potentials, the catalytic material is progressively converted into an amorphous oxide of the CoCat type; after 10 h a complete conversion is achieved. In the amorphous catalyst, the TOF per cobalt ion is relatively low, but owing to the high number of redox-active cobalt ions, the total rate of catalysis increases significantly by amorphization.

Now we will address whether enhanced activity at surface sites is a specific property of crystallite surfaces or also of relevance in amorphous materials, specifically in the CoCat formed by electrodeposition. In the experiments of Figure 6,

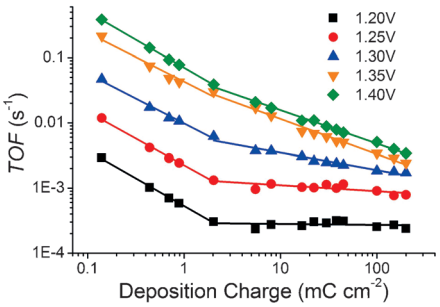

Figure 6. Turnover frequency (TOF) per cobalt ion and formed O_2 molecule for amorphous CoCat films of various thicknesses. The *x* axis indicates the deposition charge which corresponds to the amount of cobalt ions electrodeposited on an ITO electrode; a deposition charge of 10 mC corresponds to about 100 nmol cm^{-2} and to a thickness of the electrode film of about 70 nm.[8] The catalytic current was measured after equilibration for 60 s at the indicated electrode potentials (vs. NHE, pH 7); the TOF was calculated for the total amount of cobalt ions present in the catalyst film (the data relating to deposition charges ranging 2 mC to 200 mC has been discussed before[8]). The straight lines result from curve-fitting; the respective parameters are shown in Table S4. A similar thickness dependence of the catalytic current densities is observable in the amorphized Pak catalyst (Table S5 and S6).

the ratio between potential catalytic sites at the bulk-water–bulk-oxide interface (surface catalysis) and within the bulk phase of the CoCat film (volume catalysis) was altered by variation of the amount of deposited cobalt ions by more than three orders of magnitude from 140 $\mu C\,cm^{-2}$ to 200 $mC\,cm^{-2}$. For deposition of 2 $mC\,cm^{-2}$ to 200 $mC\,cm^{-2}$ and if the current density stays below the level of proton transport limitation (1.20 V and 1.25 V data points in Figure 4), the catalytic current is proportional to the number of deposited cobalt ions; consequently, the TOF per cobalt ion remains fully constant. This is explainable by equal catalytic activity throughout the bulk volume of the catalyst film.[8]

The prevalence of volume catalysis for estimated film thicknesses ranging from 15 nm (2 $mC\,cm^{-2}$) to 1.5 μm (200 $mC\,cm^{-2}$) has been reported before.[8] Herein we extended the range of deposited cobalt ions down to the level of 140 $\mu C\,cm^{-2}$, and to our surprise we find an increase in the TOF per cobalt ion by one order of magnitude. X-ray absorption spectroscopy reveals that by deposition of small amounts cobalt ions, the atomic structure and level of amorphicity of the catalytic material is not altered in any detectable way (Figure S26). Irrespective of the amount of deposited cobalt ions, the catalyst consists of cobalt oxide fragments with Co^{III} ions extensively interconnected by di-μ-oxo bridges (Figure 1 A).

The following explanation is proposed for the increased TOF at low deposition charge: For deposition of thick films (> 10 nm), catalysis within the bulk volume of the catalyst film dominates; the corresponding TOF per cobalt ion is relatively low ($10^{-3}\ s^{-1}$ at 1.25 V). At lower levels of deposited cobalt ions however, surface catalysis prevails and the corresponding TOF per cobalt ion is significantly higher than observed for volume catalysis (minimally by one order of magnitude; $10^{-2}\ s^{-1}$ at 1.25 V). This finding may or may not relate to the finding that in thin CoCat films enhanced catalysis could result from an influence of the electrode material on the electronic properties of the CoCat material.[15] Our comparison of the CoCat performance for electrodeposition on ITO, gold, or platinum did not provide evidence for a sizeable substrate influence (Figure S29).

In summary, we have shown that upon exposure to oxidizing potentials, an initially crystalline cobalt phosphate (Pak) is slowly (timescale of several hours) but eventually completely transformed into an amorphous phosphate-containing cobalt oxide (CoCat). The amorphization is coupled to catalyst activation, meaning that a sizeable increase in the total catalytic activity is observed. The electrochemical properties support that in the initial crystalline state, surface activity of the catalysts prevails, whereas amorphization results in later dominating volume activity of the bulk of the hydrated oxide material. We conclude that the differentiation between catalysis at the electrolyte exposed, "outer surface" of the oxide material and catalysis within the amorphous bulk volume of the hydrated oxide is of critical importance when discussing mechanistic aspects. The results reported herein suggest that functional investigations completed within tens of minutes indeed could probe catalysis of water oxidation at the surface of a crystalline material. However, control experiments are recommendable to assess the amorphization rate, which will likely depend on elemental composition and crystal structure, dimension of crystallites, and operation conditions (pH, electric potential, and temperature). Whether fully amorphization-resistant materials for heterogeneous water oxidation exist remains an open question.

Recently we have demonstrated the prevalence of volume catalysis in the amorphous CoCat material[8] for deposition charges ranging from 2–200 $mC\,cm^{-2}$. Now we report an increased TOF at extremely low levels of electrodeposited cobalt ions (< 1 mC). This finding suggests that also in the amorphous CoCat the rate of catalysis could be enhanced significantly at surface exposed sites or domains. This, in turn, implies that high TOF surface catalysis of water oxidation is not restricted to surface sites of crystalline material.

Surface catalysis in pristine crystalline material either could occur at open coordination sites created by termination of the crystal lattice, involving only limited surface restructur-

ing, or could involve more extended surface amorphization. The latter option needs to be taken into account seriously when discussing catalysis by crystallites, as circumstantially evidenced by the enhanced TOFs at surface exposed sites in the amorphous CoCat material. In any event, our results presented herein demonstrate that a complete picture of water oxidation catalysis requires consideration of both surface and volume catalysis, including the dynamic restructuring and transformation of the catalyst material.

Experimental Section

Pakhomovskyite was synthesized by a previously reported precipitation method (sample A).[14]

Sample B was synthesized by electrosynthesis. The cell consists of a 100 mL beaker and two squared platinum electrode (2.5 cm^2) as anode and cathode; a water bath maintained constant temperature (25 °C). The electrolysis was performed at a fixed current density (J = 0.280 A cm^{-2}) for 3 h. An Agilent E3640A 30W DC Power Supply was used. The electrodes were submerged in 100 mL of 1.40:1.50:1.00:0.10 Co/EDTA/NaH_2PO_4/Ca ratio solution at pH 8.5, at an EDTA concentration of 0.25 M. The resulting precipitate was separated by centrifugation, washed three times with purified water and dried under vacuum.

CoCat films were electrodeposited by controlled potential electrolysis at 1.05 V (vs. NHE) in a mixture of KH_2PO_4 and K_2HPO_4 electrolytes (about 0.1 M each, pH adjusted to 7) and 0.5 mM $[Co(OH_2)_6](NO_3)_2$ solution.[5b]

Further details on sample preparation, characterization, and XAS data collection are provided in the Supporting Information.

Received: September 21, 2014
Revised: November 10, 2014
Published online: January 21, 2015

Keywords: amorphization · cobalt oxide · cobalt phosphate · electrocatalysis · water oxidation

[1] a) N. S. Lewis, D. G. Nocera, *Proc. Natl. Acad. Sci. USA* **2006**, *103*, 15729 – 15735; b) T. A. Faunce, W. Lubitz, A. W. Rutherford, D. MacFarlane, G. F. Moore, P. Yang, D. G. Nocera, T. A. Moore, D. H. Gregory, S. Fukuzumi, K. B. Yoon, F. A. Armstrong, M. R. Wasielewski, S. Styring, *Energy Environ. Sci.* **2013**, *6*, 695 – 698.

[2] a) D. G. Nocera, *Inorg. Chem.* **2009**, *48*, 10001 – 10017; b) H. Dau, C. Limberg, T. Reier, M. Risch, S. Roggan, P. Strasser, *ChemCatChem* **2010**, *2*, 724 – 761; c) X. Sala, S. Maji, R. Bofill, J. García-Antón, L. Escriche, A. Llobet, *Acc. Chem. Res.* **2014**, *47*, 504 – 516.

[3] D. A. Lutterman, Y. Surendranath, D. G. Nocera, *J. Am. Chem. Soc.* **2009**, *131*, 3838 – 3839.

[4] a) M. Risch, V. Khare, I. Zaharieva, L. Gerencser, P. Chernev, H. Dau, *J. Am. Chem. Soc.* **2009**, *131*, 6936 – 6937; b) M. W. Kanan, J. Yano, Y. Surendranath, M. Dinca, V. K. Yachandra, D. G. Nocera, *J. Am. Chem. Soc.* **2010**, *132*, 13692 – 13701; c) M. Risch, K. Klingan, F. Ringleb, P. Chernev, I. Zaharieva, A. Fischer, H. Dau, *ChemSusChem* **2012**, *5*, 542 – 549.

[5] a) Y. Surendranath, M. Dinca, D. G. Nocera, *J. Am. Chem. Soc.* **2009**, *131*, 2615 – 2620; b) Y. Surendranath, M. W. Kanan, D. G. Nocera, *J. Am. Chem. Soc.* **2010**, *132*, 16501 – 16509; c) W. H. Casey, J. G. McAlpin, Y. Surendranath, M. Dinca, T. A. Stich, S. A. Stoian, D. G. Nocera, R. D. Britt, *J. Am. Chem. Soc.* **2010**, *132*, 6882 – 6883; d) E. R. Young, D. G. Nocera, V. Bulovic, *Energy Environ. Sci.* **2010**, *3*, 1726 – 1728; e) J. B. Gerken, E. C. Landis, R. J. Hamers, S. S. Stahl, *ChemSusChem* **2010**, *3*, 1176 – 1179; f) D. K. Zhong, D. R. Gamelin, *J. Am. Chem. Soc.* **2010**, *132*, 4202 – 4207; g) J. B. Gerken, J. G. McAlpin, J. Y. C. Chen, M. L. Rigsby, W. H. Casey, R. D. Britt, S. S. Stahl, *J. Am. Chem. Soc.* **2011**, *133*, 14431 – 14442; h) D. K. Bediako, B. Lassalle-Kaiser, Y. Surendranath, J. Yano, V. K. Yachandra, D. G. Nocera, *J. Am. Chem. Soc.* **2012**, *134*, 6801 – 6809; i) B. Klahr, S. Gimenez, F. Fabregat-Santiago, J. Bisquert, T. W. Hamann, *J. Am. Chem. Soc.* **2012**, *134*, 16693 – 16700.

[6] M. Risch, K. Klingan, I. Zaharieva, H. Dau, *Molecular Water Oxidation Catalysis*, Wiley, Chichester, **2014**, pp. 163 – 185.

[7] a) S. Trasatti, *J. Electroanal. Chem.* **1980**, *111*, 125 – 131; b) S. Trasatti, *Electrochim. Acta* **1984**, *29*, 1503 – 1512; c) A. Harriman, I. J. Pickering, J. M. Thomas, P. A. Christensen, *J. Chem. Soc. Faraday Trans. 1* **1988**, *84*, 2795 – 2806; d) J. Suntivich, K. J. May, H. A. Gasteiger, J. B. Goodenough, Y. Shao-Horn, *Science* **2011**, *334*, 1383 – 1385; e) L. Trotochaud, J. K. Ranney, K. N. Williams, S. W. Boettcher, *J. Am. Chem. Soc.* **2012**, *134*, 17253 – 17261; f) G. P. Gardner, Y. B. Go, D. M. Robinson, P. F. Smith, J. Hadermann, A. Abakumov, M. Greenblatt, G. C. Dismukes, *Angew. Chem. Int. Ed.* **2012**, *51*, 1616 – 1619; *Angew. Chem.* **2012**, *124*, 1648 – 1651; g) J. Landon, E. Demeter, N. İnoğlu, C. Keturakis, I. E. Wachs, R. Vasić, A. I. Frenkel, J. R. Kitchin, *ACS Catal.* **2012**, *2*, 1793 – 1801; h) D. M. Robinson, Y. B. Go, M. Mui, G. Gardner, Z. Zhang, D. Mastrogiovanni, E. Garfunkel, J. Li, M. Greenblatt, G. C. Dismukes, *J. Am. Chem. Soc.* **2013**, *135*, 3494 – 3501; i) R. D. L. Smith, M. S. Prévot, R. D. Fagan, S. Trudel, C. P. Berlinguette, *J. Am. Chem. Soc.* **2013**, *135*, 11580 – 11586; j) M. Bajdich, M. García-Mota, A. Vojvodic, J. K. Nørskov, A. T. Bell, *J. Am. Chem. Soc.* **2013**, *135*, 13521 – 13530; k) F. Calle-Vallejo, N. G. Inoglu, H.-Y. Su, J. I. Martinez, I. C. Man, M. T. M. Koper, J. R. Kitchin, J. Rossmeisl, *Chem. Sci.* **2013**, *4*, 1245 – 1249; l) M. W. Louie, A. T. Bell, *J. Am. Chem. Soc.* **2013**, *135*, 12329 – 12337.

[8] K. Klingan, F. Ringleb, I. Zaharieva, J. Heidkamp, P. Chernev, D. Gonzalez-Flores, M. Risch, A. Fischer, H. Dau, *ChemSusChem* **2014**, *7*, 1301 – 1310.

[9] S. W. Lee, C. Carlton, M. Risch, Y. Surendranath, S. Chen, S. Furutsuki, A. Yamada, D. G. Nocera, Y. Shao-Horn, *J. Am. Chem. Soc.* **2012**, *134*, 16959 – 16962.

[10] K. J. May, C. E. Carlton, K. A. Stoerzinger, M. Risch, J. Suntivich, Y.-L. Lee, A. Grimaud, Y. Shao-Horn, *J. Phys. Chem. Lett.* **2012**, *3*, 3264 – 3270.

[11] A. Indra, P. W. Menezes, I. Zaharieva, E. Baktash, J. Pfrommer, M. Schwarze, H. Dau, M. Driess, *Angew. Chem. Int. Ed.* **2013**, *52*, 13206 – 13210; *Angew. Chem.* **2013**, *125*, 13447 – 13451.

[12] a) R. K. Hocking, R. Brimblecombe, L.-Y. Chang, A. Singh, M. H. Cheah, C. Glover, W. H. Casey, L. Spiccia, *Nat. Chem.* **2011**, *3*, 461 – 466; b) M. M. Najafpour, A. N. Moghaddam, H. Dau, I. Zaharieva, *J. Am. Chem. Soc.* **2014**, *136*, 7245 – 7248; c) A. Indra, P. W. Menezes, N. Ranjbar, A. Bergmann, P. Strasser, M. Driess, *J. Am. Chem. Soc.* **2014**, *136*, 17530 – 17536.

[13] V. N. Yakovenchuk, G. Y. Ivanyuk, Y. A. Mikhailova, E. A. Selivanova, S. V. Krivovichev, *Can. Mineral.* **2006**, *44*, 117 – 123.

[14] A. Riou, Y. Cudennec, Y. Gerault, *Acta Crystallogr. Sect. C* **1989**, *45*, 1412 – 1413.

[15] B. S. Yeo, A. T. Bell, *J. Am. Chem. Soc.* **2011**, *133*, 5587 – 5593.